# Measurement of Diffractive Scattering of Photons with Large Momentum Transfer at HERA

## H1 Collaboration

## Abstract

The first measurement of diffractive scattering of quasi-real photons with large momentum transfer $\gamma p \rightarrow \gamma Y$, where $Y$ is the proton dissociative system, is made using the H1 detector at HERA. The measurement is performed for initial photon virtualities $Q^2 < 0.01 \ \text{GeV}^2$. Single differential cross sections are measured as a function of $W$, the incident photon-proton centre of mass energy, and $t$, the square of the four-momentum transferred at the proton vertex, in the range $175 < W < 247 \ \text{GeV}$ and $4 < |t| < 36 \ \text{GeV}^2$. The $W$ dependence is well described by a model based on perturbative QCD using a leading logarithmic approximation of the BFKL evolution. The measured $|t|$ dependence is harder than that predicted by the model and those observed in exclusive vector meson production.

F.D. Aaron[5,49], C. Alexa[5], V. Andreev[25], B. Antunovic[11], S. Aplin[11], A. Asmone[33],
A. Astvatsatourov[4], A. Bacchetta[11], S. Backovic[30], A. Baghdasaryan[38], P. Baranov[25,†],
E. Barrelet[29], W. Bartel[11], M. Beckingham[11], K. Begzsuren[35], O. Behnke[14], A. Belousov[25],
N. Berger[40], J.C. Bizot[27], M.-O. Boenig[8], V. Boudry[28], I. Bozovic-Jelisavcic[2], J. Bracinik[3],
G. Brandt[11], M. Brinkmann[11], V. Brisson[27], D. Bruncko[16], A. Bunyatyan[13,38], G. Buschhorn[26],
L. Bystritskaya[24], A.J. Campbell[11], K.B. Cantun Avila[22], F. Cassol-Brunner[21], K. Cerny[32],
V. Cerny[16,47], V. Chekelian[26], A. Cholewa[11], J.G. Contreras[22], J.A. Coughlan[6], G. Cozzika[10],
J. Cvach[31], J.B. Dainton[18], K. Daum[37,43], M. Deák[11], Y. de Boer[11], B. Delcourt[27],
M. Del Degan[40], J. Delvax[4], A. De Roeck[11,45], E.A. De Wolf[4], C. Diaconu[21], V. Dodonov[13],
A. Dossanov[26], A. Dubak[30,46], G. Eckerlin[11], V. Efremenko[24], S. Egli[36], A. Eliseev[25],
E. Elsen[11], S. Essenov[24], A. Falkiewicz[7], P.J.W. Faulkner[3], L. Favart[4], A. Fedotov[24],
R. Felst[11], J. Feltesse[10,48], J. Ferencei[16], L. Finke[11], M. Fleischer[11], A. Fomenko[25],
E. Gabathuler[18], J. Gayler[11], S. Ghazaryan[38], A. Glazov[11], I. Glushkov[39], L. Goerlich[7],
M. Goettlich[12], N. Gogitidze[25], M. Gouzevitch[28], C. Grab[40], T. Greenshaw[18], B.R. Grell[11],
G. Grindhammer[26], S. Habib[12,50], D. Haidt[11], M. Hansson[20], C. Helebrant[11],
R.C.W. Henderson[17], H. Henschel[39], G. Herrera[23], M. Hildebrandt[36], K.H. Hiller[39],
D. Hoffmann[21], R. Horisberger[36], A. Hovhannisyan[38], T. Hreus[4,44], M. Jacquet[27],
M.E. Janssen[11], X. Janssen[4], V. Jemanov[12], L. Jönsson[20], D.P. Johnson[4,†], A.W. Jung[15],
H. Jung[11], M. Kapichine[9], J. Katzy[11], I.R. Kenyon[3], C. Kiesling[26], M. Klein[18], C. Kleinwort[11],
T. Klimkovich[11], T. Kluge[18], A. Knutsson[11], R. Kogler[26], V. Korbel[11], P. Kostka[39],
M. Kraemer[11], K. Krastev[11], J. Kretzschmar[18], A. Kropivnitskaya[24], K. Krüger[15], K. Kutak[11],
M.P.J. Landon[19], W. Lange[39], G. Laštovička-Medin[30], P. Laycock[18], A. Lebedev[25],
G. Leibenguth[40], V. Lendermann[15], S. Levonian[11], G. Li[27], K. Lipka[12], A. Liptaj[26], B. List[12],
J. List[11], N. Loktionova[25], R. Lopez-Fernandez[23], V. Lubimov[24], A.-I. Lucaci-Timoce[11],
L. Lytkin[13], A. Makankine[9], E. Malinovski[25], P. Marage[4], Ll. Marti[11], H.-U. Martyn[1],
S.J. Maxfield[18], A. Mehta[18], K. Meier[15], A.B. Meyer[11], H. Meyer[11], H. Meyer[37], J. Meyer[11],
V. Michels[11], S. Mikocki[7], I. Milcewicz-Mika[7], F. Moreau[28], A. Morozov[9], J.V. Morris[6],
M.U. Mozer[4], M. Mudrinic[2], K. Müller[41], P. Murín[16,44], K. Nankov[34], B. Naroska[12,†],
Th. Naumann[39], P.R. Newman[3], C. Niebuhr[11], A. Nikiforov[11], G. Nowak[7], K. Nowak[41],
M. Nozicka[11], B. Olivier[26], J.E. Olsson[11], S. Osman[20], D. Ozerov[24], V. Palichik[9],
I. Panagoulias[l,11,42], M. Pandurovic[2], Th. Papadopoulou[l,11,42], C. Pascaud[27], G.D. Patel[18],
O. Pejchal[32], H. Peng[11], E. Perez[10,45], A. Petrukhin[24], I. Picuric[30], S. Piec[39], D. Pitzl[11],
R. Plačakytė[11], R. Polifka[32], B. Povh[13], T. Preda[5], V. Radescu[11], A.J. Rahmat[18], N. Raicevic[30],
A. Raspiareza[26], T. Ravdandorj[35], P. Reimer[31], E. Rizvi[19], P. Robmann[41], B. Roland[4],
R. Roosen[4], A. Rostovtsev[24], M. Rotaru[5], J.E. Ruiz Tabasco[22], Z. Rurikova[11], S. Rusakov[25],
D. Salek[32], F. Salvaire[11], D.P.C. Sankey[6], M. Sauter[40], E. Sauvan[21], S. Schmidt[11],
S. Schmitt[11], C. Schmitz[41], L. Schoeffel[10], A. Schöning[11,41], H.-C. Schultz-Coulon[15],
F. Sefkow[11], R.N. Shaw-West[3], I. Sheviakov[25], L.N. Shtarkov[25], S. Shushkevich[26], T. Sloan[17],
I. Smiljanic[2], P. Smirnov[25], Y. Soloviev[25], P. Sopicki[7], D. South[8], V. Spaskov[9], A. Specka[28],
Z. Staykova[11], M. Steder[11], B. Stella[33], U. Straumann[41], D. Sunar[4], T. Sykora[4],
V. Tchoulakov[9], G. Thompson[19], P.D. Thompson[3], T. Toll[11], F. Tomasz[16], T.H. Tran[27],
D. Traynor[19], T.N. Trinh[21], P. Truöl[41], I. Tsakov[34], B. Tseepeldorj[35,51], I. Tsurin[39], J. Turnau[7],
E. Tzamariudaki[26], K. Urban[15], A. Valkárová[32], C. Vallée[21], P. Van Mechelen[4], A. Vargas
Trevino[11], Y. Vazdik[25], S. Vinokurova[11], V. Volchinski[38], D. Wegener[8], M. Wessels[11],
Ch. Wissing[11], E. Wünsch[11], V. Yeganov[38], J. Žáček[32], J. Zálešák[31], Z. Zhang[27],
A. Zhelezov[24], A. Zhokin[24], Y.C. Zhu[11], T. Zimmermann[40], H. Zohrabyan[38], and F. Zomer[27]

1

[1] *I. Physikalisches Institut der RWTH, Aachen, Germany*[a]

[2] *Vinca Institute of Nuclear Sciences, Belgrade, Serbia*

[3] *School of Physics and Astronomy, University of Birmingham, Birmingham, UK*[b]

[4] *Inter-University Institute for High Energies ULB-VUB, Brussels; Universiteit Antwerpen, Antwerpen; Belgium*[c]

[5] *National Institute for Physics and Nuclear Engineering (NIPNE) , Bucharest, Romania*

[6] *Rutherford Appleton Laboratory, Chilton, Didcot, UK*[b]

[7] *Institute for Nuclear Physics, Cracow, Poland*[d]

[8] *Institut für Physik, TU Dortmund, Dortmund, Germany*[a]

[9] *Joint Institute for Nuclear Research, Dubna, Russia*

[10] *CEA, DSM/DAPNIA, CE-Saclay, Gif-sur-Yvette, France*

[11] *DESY, Hamburg, Germany*

[12] *Institut für Experimentalphysik, Universität Hamburg, Hamburg, Germany*[a]

[13] *Max-Planck-Institut für Kernphysik, Heidelberg, Germany*

[14] *Physikalisches Institut, Universität Heidelberg, Heidelberg, Germany*[a]

[15] *Kirchhoff-Institut für Physik, Universität Heidelberg, Heidelberg, Germany*[a]

[16] *Institute of Experimental Physics, Slovak Academy of Sciences, Košice, Slovak Republic*[f]

[17] *Department of Physics, University of Lancaster, Lancaster, UK*[b]

[18] *Department of Physics, University of Liverpool, Liverpool, UK*[b]

[19] *Queen Mary and Westfield College, London, UK*[b]

[20] *Physics Department, University of Lund, Lund, Sweden*[g]

[21] *CPPM, CNRS/IN2P3 - Univ. Mediterranee, Marseille, France*

[22] *Departamento de Fisica Aplicada, CINVESTAV, Mérida, Yucatán, México*[j]

[23] *Departamento de Fisica, CINVESTAV, México*[j]

[24] *Institute for Theoretical and Experimental Physics, Moscow, Russia*

[25] *Lebedev Physical Institute, Moscow, Russia*[e]

[26] *Max-Planck-Institut für Physik, München, Germany*

[27] *LAL, Univ Paris-Sud, CNRS/IN2P3, Orsay, France*

[28] *LLR, Ecole Polytechnique, IN2P3-CNRS, Palaiseau, France*

[29] *LPNHE, Universités Paris VI and VII, IN2P3-CNRS, Paris, France*

[30] *Faculty of Science, University of Montenegro, Podgorica, Montenegro*[e]

[31] *Institute of Physics, Academy of Sciences of the Czech Republic, Praha, Czech Republic*[h]

[32] *Faculty of Mathematics and Physics, Charles University, Praha, Czech Republic*[h]

[33] *Dipartimento di Fisica Università di Roma Tre and INFN Roma 3, Roma, Italy*

[34] *Institute for Nuclear Research and Nuclear Energy, Sofia, Bulgaria*[e]

[35] *Institute of Physics and Technology of the Mongolian Academy of Sciences , Ulaanbaatar, Mongolia*

[36] *Paul Scherrer Institut, Villigen, Switzerland*

[37] *Fachbereich C, Universität Wuppertal, Wuppertal, Germany*

[38] *Yerevan Physics Institute, Yerevan, Armenia*

[39] *DESY, Zeuthen, Germany*

[40] *Institut für Teilchenphysik, ETH, Zürich, Switzerland*[i]

[41] *Physik-Institut der Universität Zürich, Zürich, Switzerland*[i]

[42] *Also at Physics Department, National Technical University, Zografou Campus, GR-15773 Athens, Greece*

# 1  Introduction

The study at the $ep$ collider HERA of exclusive diffractive processes in the presence of a hard scale has provided insight into the parton dynamics of the diffractive exchange. The four-momentum squared transferred at the proton vertex, $t$, provides a relevant scale to investigate the application of perturbative Quantum Chromodynamics (pQCD) for $|t| \gg \Lambda_{\mathrm{QCD}}^2$ [1]. In this Letter, the first measurement at large $t$ ($|t| > 4$ GeV$^2$) of diffractive photon-proton scattering, $\gamma p \to \gamma Y$, where $Y$ is the proton dissociative system, is presented. The measurement is performed at HERA by studying the reaction $e^+ p \to e^+ \gamma Y$ in the photoproduction regime with a large rapidity gap between the final state photon and the proton dissociative system $Y$ (as illustrated in figure 1a). The centre of mass energy of the system formed by the exchanged photon and proton is in the range $175 < W < 247$ GeV. This process constitutes an extension of Deeply Virtual Compton Scattering [2] into the large $|t|$ and small $Q^2$ regime.

Diffractive photon scattering can be modelled in the proton rest frame by the fluctuation of the incoming photon into a $q\bar{q}$ pair at a long distance from the proton target. The $q\bar{q}$ pair is then involved in a hard interaction with the proton via the exchange of a colour singlet state. In the leading logarithmic approximation (LLA), the colour singlet exchange is modelled by the effective exchange of a gluon ladder (figure 1b). For sufficiently low values of Bjorken $x$ (i.e. large values of $W$), the BFKL [3] approach is expected to be appropriate for describing the gluon ladder. In the LLA BFKL model the gluon ladder couples to a single parton (predominantly a gluon) within the proton. The cross section depends therefore linearly on the parton distribution in the proton. Due to the quasi-real nature of the incoming photon ($Q^2 < 0.01$ GeV$^2$), the transverse momentum of the final state photon, $P_T^\gamma$, is entirely transferred by the gluon ladder to the parton in the proton. The separation in rapidity between the parton scattered by the gluon ladder and the final state photon is given by $\Delta\eta \simeq \log(\hat{s}/(P_T^\gamma)^2)$, where $\hat{s}$ is the invariant mass of the system formed by the incoming photon and the struck parton. The proton remnant and the struck parton hadronise through fragmentation processes to form the hadronic system $Y$. Assuming parton-hadron duality, hadrons originating from the struck parton correspond to the particles with the largest transverse momenta and hence are the closest in rapidity to the scattered photon.

The present analysis complements the measurements of exclusive production of $\rho, \phi$ and $J/\psi$ mesons at large $|t|$ [4–7]. The measured $W$ and $t$ dependences of their cross sections were found to be in agreement with LLA BFKL based calculations [8–12]. For the process studied here, theoretical calculations are simplified by the absence of a vector meson wave function: the only non-perturbative part of the calculation is the parton distribution functions of the proton. However, the cross section is suppressed relative to that of vector meson production by the electromagnetic coupling of the $q\bar{q}$ pair to the final state photon, making the measurement more challenging.

In the following, measurements of the photon-proton cross sections are presented as a function of $W$ and differentially in $|t|$ and are compared to predictions based on LLA BFKL calculations [12].
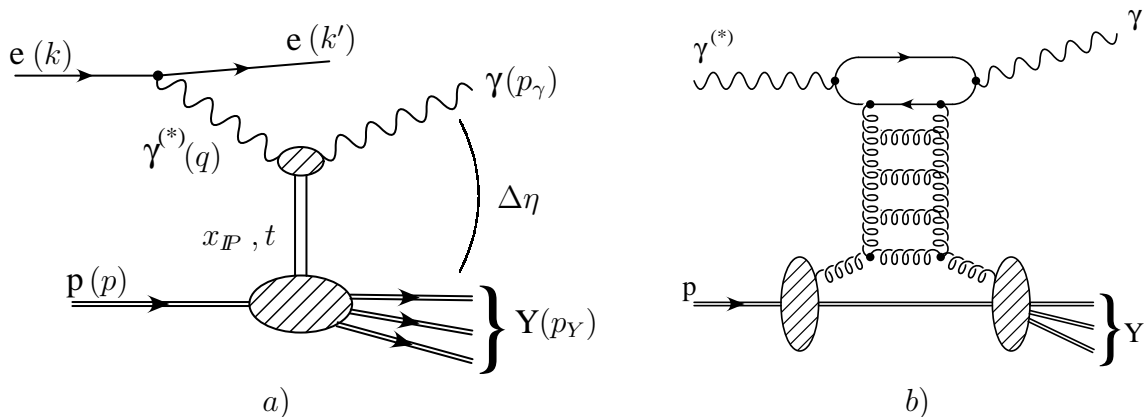
Figure 1: a) Schematic illustration of the $ep \rightarrow e\gamma Y$ process. b) Illustration of the $\gamma^{(*)}p \rightarrow \gamma Y$ process in a LLA BFKL approach.

## 2 The H1 Detector

A detailed description of the H1 detector can be found elsewhere [13]. The following briefly describes the detector components relevant to this analysis. A right handed coordinate system is defined with the origin at the nominal $ep$ interaction vertex, such that the positive $z$ axis (forward direction) corresponds to the direction of the outgoing proton beam. The polar angle $\theta$ and transverse momentum $P_T$ are defined with respect to the $z$ axis. The pseudorapidity is defined as $\eta = -\ln \tan(\theta/2)$.

A liquid argon (LAr) calorimeter covers the polar angle range $4° < \theta < 154°$ with full azimuthal coverage. The LAr calorimeter consists of both an electromagnetic section and a hadronic section. The energy resolution for single particles measured in a test beam is $\sigma_E/E = 12\%/\sqrt{E/\text{GeV}} \oplus 1\%$ for electrons and $\sigma_E/E = 50\%/\sqrt{E/\text{GeV}} \oplus 2\%$ for hadrons [14]. The polar angle region $153° < \theta < 177°$ is covered by a lead-scintillating fibre calorimeter, the SpaCal [15], with both electromagnetic and hadronic sections. The SpaCal has an energy resolution for electromagnetic showers of $\sigma_E/E = 7\%/\sqrt{E/\text{GeV}} \oplus 1\%$.

Charged particles are detected in the polar angle ranges $15° < \theta < 165°$ by the Central Track Detector (CTD) and $5° < \theta < 25°$ by the Forward Track Detector (FTD). The CTD comprises two large cylindrical jet drift chambers, providing precise track measurements in the $r - \phi$ plane, supplemented by two $z$-chambers and two multi-wire proportional chambers arranged concentrically around the beam-line. The CTD is complemented by a silicon vertex detector [16] covering the range $30° < \theta < 150°$. The FTD consists of layers of planar and radial drift chambers to provide measurement of the $\theta$ and $\phi$ angles of forward tracks, respectively. The trackers and the calorimeters are operated within a solenoidal magnetic field of $1.16$ T.

The luminosity is determined from the rate of Bethe-Heitler events, $ep \rightarrow ep\gamma$, measured using a Čerenkov crystal calorimeter, the Photon Detector (PD), situated near the HERA beam pipes at $z = -103$ m. A second Čerenkov crystal calorimeter, the Electron Tagger (ET), with an energy resolution of $\sigma_E/E = 17\%/\sqrt{E/\text{GeV}} \oplus 1\%$, is located at $z = -33$ m. The ET measures the energy of the positron when scattered through an angle of less than $5$ mrad in the energy range $8 < E < 20$ GeV. The detection of the scattered positron in the ET ensures that the exchanged photon is quasi-real with $Q^2 < 0.01$ GeV$^2$.

# 3 Event Kinematics and Selection

Following the notation introduced in figure 1a, the scattering process, $e^+ p \rightarrow e^+ \gamma Y$, is described by the usual Deep Inelastic Scattering (DIS) kinematic variables:

$$Q^2 = -q^2 = -(k' - k)^2, \qquad y = \frac{p \cdot q}{p \cdot k},$$

where $k$, $p$, $k'$ and $q$ are the four-momentum of the incoming positron, the incoming proton, the scattered positron and the exchanged photon, respectively. The variable $Q^2$ is the virtuality of the exchanged photon and $y$ is the inelasticity of the $ep$ interaction, corresponding to the relative energy loss of the scattered positron in the proton rest frame. The $ep$ centre of mass energy squared is given by $s = (k + p)^2$ and the $\gamma p$ centre of mass energy squared is $W^2 = (q + p)^2 \simeq ys$. In addition, the longitudinal momentum fraction of the diffractive exchange (called the Pomeron in the Regge model [17]) with respect to the proton is defined as:

$$x_{I\!P} = \frac{q \cdot (p - p_Y)}{q \cdot p},$$

where $p_Y$ is the four-momentum of the $Y$ system. The elasticity of the $\gamma p$ interaction, which can be seen as the fractional energy of the exchanged photon transferred to the final state photon, is given by $1 - y_{I\!P}$, where:

$$y_{I\!P} = \frac{p \cdot (q - p_\gamma)}{p \cdot q},$$

$p_\gamma$ being the four-momentum of the final state photon. Finally the square of the four-momentum transfer across the diffractive exchange is given by:

$$t = (q - p_\gamma)^2 = (p - p_Y)^2.$$

The data used in this analysis were collected with the H1 detector during the $1999 - 2000$ running period, when positrons of energy $E_e = 27.6$ GeV collided with protons of energy $E_p = 920$ GeV in the HERA accelerator. The data sample corresponds to an integrated luminosity of $46.2$ pb$^{-1}$. More details on the present analysis can be found in [18].

The data were recorded using a combination of two triggers. Both triggers select an electromagnetically interacting particle in the SpaCal which corresponds to the scattered photon candidate. One of the triggers requires in addition an energy deposit in the ET, corresponding to the scattered positron. The effective trigger efficiency, including time dependent downscale factors, amounts to approximately $50\%$.

The reconstruction of the kinematic quantities used in the following are approximations valid in the limit of small scattering angles of the positron and small transverse momentum of the $Y$ system compared to its longitudinal momentum. The quantity $y$, and hence $W$, is calculated from the scattered positron energy, $E_{e'}$, measured in the ET using the relation $y = 1 - E_{e'}/E_e$. The relative resolution of $W$ is $4\%$. To avoid regions of low ET acceptance, the energy of the scattered positron is limited to $11 < E_{e'} < 19$ GeV, corresponding to $175 < W < 247$ GeV. In addition, to suppress backgrounds from processes occurring in coincidence

with Bethe-Heitler events, it is required that no energy deposits above the noise threshold are measured in the PD.

Photon candidates are selected from energy clusters with small radii detected in the electromagnetic section of the SpaCal. If significant energy is measured behind the cluster in the hadronic section of the SpaCal, the event is rejected. Events with more than one cluster above the noise level in the SpaCal are also rejected. To reduce the background from charged particles, the cluster of the photon candidate must have no associated track in the CTD. The photon candidates are furthermore required to have an energy $E_\gamma > 8$ GeV and a transverse momentum $P_T^\gamma > 2$ GeV.

The hadronic final state $Y$ is reconstructed using a combination of tracking and calorimetric information. The difference between the total energy $E$ and the longitudinal component of the total momentum $P_z$, as calculated from the scattered positron, the final state photon and the hadronic system $Y$, is restricted to $49 < \Sigma(E - P_z) < 61$ GeV. This requirement suppresses non-$ep$ induced background and background due to the overlap during the same bunch crossing of a Bethe-Heitler event with a DIS event. For a fully contained $ep$ event the relation $\Sigma(E - P_z) = 2E_e = 55$ GeV holds.

In the case that charged particles from the final state are detected by the tracking detector, allowing the primary vertex to be reconstructed, the $z$ coordinate of the vertex has to satisfy $|z| < 35$ cm. For $25\%$ of the selected events, all charged particles of the final state lie outside the detector acceptance and no event vertex is reconstructed. In this case, the time averaged vertex position is used for the kinematic reconstruction.

The kinematic variable $|t|$ is reconstructed as:

$$|t| = (P_T^\gamma)^2,$$

with a relative resolution of $11\%$. The longitudinal momentum fraction of the diffractive exchange with respect to the proton is reconstructed using the formula:

$$x_{I\!P} \simeq \frac{(E + P_z)_\gamma}{2E_p},$$

where $(E + P_z)_\gamma$ is the sum of the energy and longitudinal momentum of the final state photon. The event inelasticity of the $\gamma p$ interaction is reconstructed as:

$$y_{I\!P} \simeq \frac{\sum_Y (E - P_z)}{2(E_e - E_{e'})},$$

where the summation is performed on all detected hadronic final state particles in the event, i.e. all measured particles except the scattered positron and the final state photon. This reconstruction method has the advantage that the loss of particles along the forward beam pipe only has a marginal effect on the reconstruction of $y_{I\!P}$. Diffractive events are selected by requiring that $y_{I\!P} < 0.05$. The cut value ensures a large pseudorapidity gap, $\Delta\eta$, between the photon and the proton dissociative system $Y$, since $y_{I\!P} \simeq e^{-\Delta\eta}$.

Finally, to reduce contamination of the signal by non-diffractive background, it is required that the difference in pseudorapidity between the photon and the closest final state hadron satisfies $\Delta\eta > 2$. This rapidity gap is inferred from the absence of activity in the relevant detector

parts, i.e. absence of any track or a cluster of energy deposits above the noise threshold of $400$ MeV in the LAr calorimeter. [1]

After applying all selection criteria, 240 events remain in the data sample.

# 4 Monte Carlo Simulations and Comparison to Data

Monte Carlo (MC) simulations are used to correct the data for effects of detector acceptance and efficiency, to estimate the background and to compare model predictions to the data. All generated MC events are passed through the full GEANT [19] based simulation of the H1 detector and are reconstructed using the same analysis chain as is used for the data.

The HERWIG 6.4 [20] MC event generator is used to simulate the diffractive high $|t|$ photon scattering using the LLA BFKL model [10–12]. At leading logarithmic accuracy there are two independent free parameters in the BFKL calculation: the value of the strong coupling $\alpha_s$ and the scale, $c$, which defines the leading logarithms in the expansion of the BFKL amplitude, $\ln(W^2/(c\,|t|))$. In exclusive production of vector mesons, the scale parameter $c$ is related to the vector meson mass. In the case of diffractive photon scattering, the unknown scale results in the absence of a prediction for the normalisation of the cross section [21]. In the calculations considered here [12], the running of $\alpha_s$ as a function of the scale is ignored. In order to distinguish the $\alpha_s$ parameter of the LLA BFKL model from the usual strong coupling constant this parameter will henceforth be referred to as $\alpha_s^{BFKL}$. The choice of $\alpha_s^{BFKL} = 0.17$ is used for the simulation in this Letter.

In the asymptotic approximation of the calculations [12], the W distribution follows a power-law:

$$\sigma(W) \sim W^{4\omega_0},$$

where the exponent, also called the Pomeron intercept, is given directly by the choice of $\alpha_s^{BFKL}$ with $\omega_0 = (3\alpha_s^{BFKL}/\pi)\,4\,\ln 2$. Using the HERWIG simulation this approximation is found to be justified given the current experimental statistical precision. The LLA BFKL model predicts an approximate power-law behaviour for the $t$ dependence of the cross section of the form $d\sigma/d|t| \sim |t|^{-n}$, where $n$, also predicted by the model, depends only on the parton density functions (PDFs) of the proton and the value of $\alpha_s^{BFKL}$. Running coupling effects, not considered here, would in principle allow $n$ to depend on $t$.

The GRV94 PDFs [22] are used for the proton PDFs in the HERWIG prediction. A comparison with the CTEQ5 [23] and MRST PDFs [24] shows little dependence of the HERWIG prediction on the input proton PDFs.

In order to describe the data, the $t$ dependence of the diffractive photon scattering simulated using HERWIG (predicting a value of $n = 3.31$ for $\alpha_s^{BFKL} = 0.17$) was weighted by a factor $|t|^{0.73}$, i.e. the $|t|$ power is modified from $-3.31$ to $-2.58$. This weighted HERWIG prediction is used to correct the data for resolution and acceptance effects.

---

[1]The noise level of the LAr calorimeter is about 10 MeV per cell and the average number of cells per cluster is typically 60.

Possible sources of background are estimated using MC simulations. The background from inclusive diffractive photoproduction events ($ep \to eXY$, where the two hadronic final states are separated by a rapidity gap) is simulated using the PHOJET MC event generator [25]. This background contributes when a single electromagnetic particle fakes the photon candidate in the SpaCal. It is estimated to amount to $3\%$ of the measured cross section. The background from electron pair production ($ep \to ee^+e^-X$) is modelled using the GRAPE event generator [26]. This process contributes to the selection if one lepton is detected in the ET, a second lepton fakes the photon within the SpaCal and the remaining lepton escapes detection. This background contributes $4\%$ of the measured cross section.

In order to investigate the background from high $|t|$ diffractive exclusive $\omega$ production, where the $\omega$ decays through the $\pi^+\pi^-\pi^0$ or $\pi^0\gamma$ channel, a sample was generated using the DIFFVM Monte Carlo generator [27]. The contribution from this background process is found to be negligible. The background from DIS events, in which the scattered positron fakes the photon candidate and an overlapping photoproduction or Bethe-Heitler event gives a positron detected in the ET, has been studied and was also found to be negligible.

In figure 2 the data, corrected for trigger efficiency, are compared to the Monte Carlo simulations. The background predictions from GRAPE and PHOJET are normalised to the integrated luminosity of the data sample. The weighted HERWIG prediction is normalised to the number of events obtained after the subtraction of the predicted background from the data. A good description of the data by the combined Monte Carlo simulations is observed.

# 5   Cross Section Measurement

The $ep \to e\gamma Y$ differential cross sections are defined using the formula:

$$\frac{\mathrm{d}^2\sigma_{ep \to e\gamma Y}}{\mathrm{d}W\,\mathrm{d}t} = \frac{N_{data} - N_{bgr}}{\mathcal{L}A\,\Delta W\,\Delta t},$$

where $N_{data}$ is the number of observed events corrected for trigger efficiency, $N_{bgr}$ the expected contribution from background events as estimated using the PHOJET and GRAPE Monte Carlos simulations, $\mathcal{L}$ the integrated luminosity, $A$ the signal acceptance and $\Delta W$ and $\Delta t$ the bin widths in $W$ and $t$, respectively. The acceptance, estimated using the weighted HERWIG simulation, is the ratio of the number of events accepted after reconstruction to the number of events generated in the defined phase space on hadron level. It accounts for all detector effects, including bin-to-bin migrations, as well as geometrical acceptance and detector efficiencies. QED radiative correction effects are estimated to be less than $1\%$ [28] and are neglected.

The $\gamma p \to \gamma Y$ differential cross section is then extracted from the $ep$ cross section using:

$$\frac{\mathrm{d}^2\sigma_{ep \to e\gamma Y}}{\mathrm{d}W\,\mathrm{d}t} = \Gamma(W)\,\frac{\mathrm{d}\sigma_{\gamma p \to \gamma Y}}{\mathrm{d}t}(W), \tag{1}$$

where the photon flux, $\Gamma(W)$, is integrated over the range $Q^2 < 0.01$ GeV$^2$ according to the modified Weizsäcker-Williams approximation [29]. The $\gamma p$ cross section is obtained by modelling $\sigma_{\gamma p \to \gamma Y}$ as a power-law in $W$, whose parameters are iteratively adjusted to reproduce the

measured $W$ dependence of the $ep$ cross section. The differential $\gamma p$ cross section in $|t|$ is then extracted from the $ep$ cross section by correcting for the effect of the photon flux over the visible $W$ range ($175 < W < 247$ GeV). The $\gamma p$ cross section as a function of $W$ is obtained by first integrating equation (1) over the $|t|$ range, and then correcting for the effect of the photon flux in each bin in $W$. More details on the extraction procedure of the $\gamma p$ cross section can be found in [18].

The systematic error on the measurement stems from experimental uncertainties and from model dependences. They are calculated using the weighted HERWIG simulation of the signal process. The sources of systematic error are listed below. For each of them the typical effect on the cross section measurement is indicated.

The experimental systematic errors are:

- The energy scale uncertainty of $\pm 1\%$ for an electromagnetic cluster measured by the SpaCal gives errors in the range of $2\%$ to $4\%$.

- The uncertainty of $\pm 2.5$ mrad for the measurement of the photon candidate polar angle results in an error of up to $3\%$.

- The hadronic final state energy scale uncertainty of $\pm 4\%$ leads to an error of less than $1.5\%$.

- The energy scale uncertainty of $\pm 1.5\%$ of the ET produces an error ranging from $1\%$ in the highest $|t|$ bin to $10\%$ in the lowest $W$ bin.

- The uncertainty of $\pm 25\%$ on the noise threshold from the calorimeters gives an error varying from $5\%$ at low $|t|$ to $11\%$ at the highest $|t|$ value.

- The luminosity is measured with an accuracy of $\pm 1.5\%$ which enters as an overall normalisation uncertainty.

The systematic errors due to uncertainty of model parameters are:

- The uncertainty due to the $x_{I\!P}$ dependence, estimated by weighting the $x_{I\!P}$ distribution by the form $(1/x_{I\!P})^{\pm 0.4}$, yields an error varying from $3\%$ in the central $|t|$ bin up to $9\%$ in the lowest $W$ bin. This weight would correspond to changing $\alpha_s^{BFKL}$ to the values $0.02$ and $0.31$.

- The uncertainty due to the $|t|$ dependence, estimated by weighting the $|t|$ distribution by the form $(1/|t|)^{\pm 0.2}$, leads to an error ranging from $1.5\%$ to $4\%$.

- The uncertainty in the modelling of the proton remnant system $Y$, estimated by weighting the $M_Y$ distribution by the form $(1/M_Y^2)^{\pm 0.3}$, results in a typical error of $1\%$ to $4\%$.

- The uncertainty of $100\%$ assumed on the normalisation of the subtracted inclusive diffractive background (from the PHOJET Monte Carlo simulation) leads to an error of approximately $3\%$ in the highest $W$ bins decreasing to $1\%$ in the highest $|t|$ bin.

- The propagation of the uncertainty on the power-law parameter $\delta$ in the $\gamma p$ cross section extraction procedure leads to an error of $4\%$ on $\mathrm{d}\sigma_{\gamma p \to \gamma Y}/\mathrm{d}|t|$, independent of $|t|$, and is below $1\%$ on $\sigma_{\gamma p \to \gamma Y}$.

The uncertainty on the PHOJET MC normalisation and the model uncertainties from the unknown $x_{I\!\!P}$, $|t|$ and $M_Y$ dependences are estimated from data comparisons and defined by the range where the model describes the data. Each source of systematic error is varied in the weighted HERWIG Monte Carlo within its uncertainty. In each measurement bin, the corresponding deviation of the normalised cross section from the central value is taken as systematic error. The total systematic error is obtained by adding the individual contributions in quadrature, on a bin-by-bin basis. The largest systematic error on the cross sections comes from the uncertainty on the $x_{I\!\!P}$ and $M_Y$ dependences in the MC simulation. The total systematic error on the $W$ dependence of the cross section varies from $10\%$ in the central bins to $17\%$ in the lowest bin. The systematic error on the $|t|$ dependence of the cross section varies from $8\%$ in the lowest bin to $14\%$ in the highest bin. An additional global uncertainty of $4\%$ arises from the $\gamma p$ cross section extraction procedure. The total systematic errors are comparable to or smaller than the statistical errors.

# 6  Results

The cross sections measured for the domain $175 < W < 247$ GeV, $4 < |t| < 36$ GeV$^2$, $y_{I\!\!P} < 0.05$ and $Q^2 < 0.01$ GeV$^2$ are presented in table 1.

The $\gamma p \to \gamma Y$ cross section as a function of $W$ is shown in figure 3. A power-law dependence of the form $\sigma \sim W^\delta$ is fitted to the measured cross section. The fit yields $\delta = 2.73 \pm 1.02$ (stat.)$^{+0.56}_{-0.78}$ (syst.) with $\chi^2/\mathrm{n.d.f.} = 2.7/2$. The contributions from the systematic errors are calculated by shifting the data points according to each source of uncertainty, taking correlations into account, and repeating the fit. The errors are then added in quadrature to obtain the total systematic error.

The steep rise of the cross section with $W$ is usually interpreted as an indication of the presence of a hard sub-process in the diffractive interaction and of the applicability of perturbative QCD. The present $\delta$ value, measured at an average $|t|$ value of $6.1$ GeV$^2$, is compatible with that measured by H1 in diffractive $J/\psi$ photoproduction of $\delta = 1.29 \pm 0.23(\mathrm{stat.}) \pm 0.16(\mathrm{syst.})$ [6] at an average $|t|$ of $6.9$ GeV$^2$. The Pomeron intercepts associated with these $\delta$ values correspond to the strongest energy dependences measured in diffractive processes.

The $\gamma p$ cross section differential in $|t|$, at $W = 219$ GeV, is shown in figure 4. Figure 4 also shows the comparison of the cross section to a fit of the form $\mathrm{d}\sigma/\mathrm{d}t \sim |t|^{-n}$. The fit result is $n = 2.60 \pm 0.19$ (stat.)$^{+0.03}_{-0.08}$ (syst.) with $\chi^2/\mathrm{n.d.f.} = 1.6/1$. The $|t|$ dependence is harder than that measured by H1 in the diffractive photoproduction of $J/\psi$ mesons at large $|t|$ [6] corresponding to $n = 3.78 \pm 0.17(\mathrm{stat.}) \pm 0.06(\mathrm{syst.})$.

In figures 3 and 4 the measured cross sections are compared to predictions of the LLA BFKL model, using the HERWIG Monte Carlo, as described in section 4, with no $|t|$ weighting. The predictions are normalised to the integrated measured cross section, as the normalisation is

11

| H1 measured $ep \rightarrow e\gamma Y$ cross sections | | | | |
|---|---|---|---|---|
| $W$ [GeV] | $W$ range [GeV] | $\mathrm{d}\sigma_{ep\rightarrow e\gamma Y}/\mathrm{d}W$ [pb/GeV] | $\Gamma(W)$ [GeV$^{-1}$] | $\sigma_{\gamma p\rightarrow \gamma Y}$ [nb] |
| 185 | 175 − 193 | $0.414 \pm 0.069 \pm 0.072$ | 0.0565 | $2.02 \pm 0.34 \pm 0.35$ |
| 202 | 193 − 211 | $0.318 \pm 0.046 \pm 0.033$ | 0.0431 | $1.86 \pm 0.27 \pm 0.19$ |
| 220 | 211 − 229 | $0.434 \pm 0.062 \pm 0.051$ | 0.0328 | $3.06 \pm 0.44 \pm 0.36$ |
| 240 | 229 − 247 | $0.404 \pm 0.080 \pm 0.044$ | 0.0246 | $3.48 \pm 0.69 \pm 0.38$ |
| $\lvert t \rvert$ [GeV$^2$] | $\lvert t \rvert$ range [GeV$^2$] | $\mathrm{d}\sigma_{ep\rightarrow e\gamma Y}/\mathrm{d}\lvert t \rvert$ [pb/GeV$^2$] | $\Gamma(W = 219 \text{ GeV})$ [GeV$^{-1}$] | $\mathrm{d}\sigma_{\gamma p\rightarrow \gamma Y}/\mathrm{d}\lvert t \rvert$ [pb/GeV$^2$] |
| 6 | 4.0 − 8.3 | $4.04 \pm 0.42 \pm 0.36$ | 0.0333 | $401 \pm 41 \pm 36$ |
| 12 | 8.3 − 17.3 | $0.58 \pm 0.08 \pm 0.06$ | 0.0333 | $57.8 \pm 8.1 \pm 6.2$ |
| 25 | 17.3 − 36.0 | $0.13 \pm 0.03 \pm 0.02$ | 0.0333 | $12.5 \pm 3.1 \pm 1.8$ |

Table 1: The cross sections for the processes $ep \rightarrow e\gamma Y$ and the $\gamma p \rightarrow \gamma Y$, measured in the range $y_{I\!P} < 0.05$ and $Q^2 < 0.01$ GeV$^2$. The upper part of the table presents the measured cross sections for different values of $W$ at an average $\langle \lvert t \rvert \rangle = 6.1$ GeV$^2$. The lower table presents the measured cross sections differential in $\lvert t \rvert$ at $W = 219$ GeV. The first errors are statistical, the second systematic. The photon flux $\Gamma$ and corresponding ranges in $W$ and $\lvert t \rvert$ used for the measurements are also given.

not predicted by the LLA BFKL calculation [21]. The $W$ dependence of the cross section is well described by the LLA BFKL prediction, as shown in figure 3. The sensitivity of the measurement to the free parameter $\alpha_s^{BFKL}$ in the theoretical prediction is illustrated in figures 3 and 4. Using $\delta = 4\,\omega_0 = 4\,(3\alpha_S^{Fit}/\pi)\,4\,\ln 2$, the measured $W$ dependence leads to $\alpha_S^{Fit} = 0.26 \pm 0.10$ (stat.)$^{+0.05}_{-0.07}$ (syst.). Predictions are shown in figure 3 for the values $\alpha_s^{BFKL} = 0.14$ and 0.37. The LLA BFKL curve corresponding to $\alpha_s^{BFKL} = 0.26$ coincides with the solid fit line.

Previous measurements of diffractive scattering at HERA are well described by BFKL predictions with $\alpha_s^{BFKL}$ values similar to the value measured in this Letter. ZEUS measurements of exclusive $\rho, \phi$ and $J/\psi$ production at large $\lvert t \rvert$ are best described with the value of $\alpha_s^{BFKL} = 0.20$ [4]. The H1 measurement of high $\lvert t \rvert$ $\rho$ production [5] is compatible with $\alpha_s^{BFKL} = 0.20$ and the H1 measurement of high $\lvert t \rvert$ $J/\psi$ production [6] is described using $\alpha_s^{BFKL} = 0.18$. The LLA BFKL prediction with $\alpha_s^{BFKL} = 0.17$ gives a good description of the double dissociation process with a rapidity gap between jets measured by H1 [30]. Events with rapidity gaps between jets were also measured by ZEUS [31] and are found to be compatible with a model which uses $\alpha_s^{BFKL} = 0.11$. Note, however, that for these measurements the hard scale, corresponding to the jet transverse momentum squared, is of the order of or larger than 20 GeV$^2$.

As shown in figure 4, the LLA BFKL calculation for $\alpha_s^{BFKL} = 0.14, 0.26$ and 0.37, all of which give a reasonable description of the $W$ dependence, predict steeper $\lvert t \rvert$ distributions than is measured in the data. The same effect cannot be established for the exclusive $\rho$ measurement [5], where the measured $t$ range is limited to $\lvert t \rvert < 8$ GeV$^2$, although an underestimate of the cross section was observed at the largest values of $\lvert t \rvert$. The present situation is in contrast with the analysis of $J/\psi$ production [4, 6], where the $\lvert t \rvert$ dependence was found to be well described

by the LLA BFKL prediction over a similar range in $t$.

# 7 Conclusions

Using the H1 detector, diffractive photon scattering, $\gamma p \rightarrow \gamma Y$, where the final state photon carries a large transverse momentum and is well separated from the proton dissociative system $Y$, is measured for the first time at HERA. The measurement provides a unique test of the underlying QCD dynamics of the diffractive exchange.

Cross sections are presented as a function of $W$ and differentially in $|t|$. A fit of the form $W^\delta$ performed on the cross section gives $\delta = 2.73 \pm 1.02 \text{ (stat.)}^{+0.56}_{-0.78} \text{ (syst.)}$. This strong energy dependence is compatible with that measured for the exclusive diffractive $J/\psi$ production at high $|t|$. A fit of the form $|t|^{-n}$ yields $n = 2.60 \pm 0.19 \text{ (stat.)}^{+0.03}_{-0.08} \text{ (syst.)}$, corresponding to a harder $|t|$ dependence of the cross section than measured for high $|t|$ diffractive $J/\psi$ production.

The measured cross sections are compared to the predictions of an LLA BFKL model. A good description of the $W$ dependence of the cross section is found, whereas the LLA BFKL model predicts a $|t|$ dependence that is too soft and hence unable to describe the data.

# Acknowledgements

# References

[1] J. R. Forshaw and P. J. Sutton, Eur. Phys. J. C **1** (1998) 285 [hep-ph/9703225].

[2] F. D. Aaron *et al.* [H1 Collaboration], Phys. Lett. B **659** (2008) 796 [arXiv:0709.4114 [hep-ex]].

[3] E. A. Kuraev, L. N. Lipatov and V. S. Fadin, Sov. Phys. JETP **45** (1977) 199 [Zh. Eksp. Teor. Fiz. **72** (1977) 377];
I. I. Balitsky and L. N. Lipatov, Sov. J. Nucl. Phys. **28** (1978) 822 [Yad. Fiz. **28** (1978) 1597];
L. N. Lipatov, Sov. Phys. JETP **63** (1986) 904 [Zh. Eksp. Teor. Fiz. **90** (1986) 1536].

[4] S. Chekanov *et al.* [ZEUS Collaboration], Eur. Phys. J. C **26** (2003) 389 [hep-ex/0205081].

[5] A. Aktas *et al.* [H1 Collaboration], Phys. Lett. B **638** (2006) 422 [hep-ex/0603038].

[6] A. Aktas *et al.* [H1 Collaboration], Phys. Lett. B **568** (2003) 205 [hep-ex/0306013].

[7] S. Chekanov *et al.* [ZEUS Collaboration], Eur. Phys. J. C **24** (2002) 345 [hep-ex/0201043].

[8] I. F. Ginzburg and D. Y. Ivanov, Phys. Rev. D **54** (1996) 5523 [hep-ph/9604437].

[9] I. F. Ginzburg, S. L. Panfil and V. G. Serbo, Nucl. Phys. B **284** (1987) 685.

[10] D. Y. Ivanov and M. Wüsthoff, Eur. Phys. J. C **8** (1999) 107 [hep-ph/9808455].

[11] N. G. Evanson and J. R. Forshaw, Phys. Rev. D **60** (1999) 034016 [hep-ph/9902481].

[12] B. E. Cox and J. R. Forshaw, J. Phys. G **26** (2000) 702 [hep-ph/9912486].

[13] I. Abt *et al.* [H1 Collaboration], Nucl. Instrum. Meth. A **386** (1997) 310 and 348.

[14] B. Andrieu *et al.* [H1 Calorimeter Group], Nucl. Instrum. Meth. A **350** (1994) 57.

[15] R. D. Appuhn *et al.* [H1 SPACAL Group Collaboration], Nucl. Instrum. Meth. A **386** (1997) 397.

[16] D. Pitzl *et al.*, Nucl. Instrum. Meth. A **454** (2000) 334 [hep-ex/0002044].

[17] E. Feinberg and I. Pomeranchuk, Suppl. Nuovo Cimento **3** (1956) 652;
V. Gribov, JETP Lett. **41** (1961) 667.

[18] T. Hreus, Ph.D. Thesis, Université Libre de Bruxelles and Pavol Jozef Šafárik University (2008), available at http://www-h1.desy.de/psfiles/theses/h1th-495.pdf;
M. Beckingham, Ph.D. Thesis, "Diffractive Photoproduction of High $p_T$ Photons at HERA", University of Manchester (2003), available at http://www-h1.desy.de/psfiles/theses/h1th-434.ps.

[19] R. Brun *et al.*, "Geant3," CERN-DD/EE/84-1.

[20] G. Marchesini *et al.*, Comput. Phys. Commun. **67** (1992) 465.

[21] B. Cox, J. R. Forshaw and L. Lönnblad, JHEP **9910** (1999) 023 [hep-ph/9908464].

[22] M. Glück, E. Reya and A. Vogt, Z. Phys. C **67** (1995) 433.

[23] H. L. Lai *et al.* [CTEQ Collaboration], Eur. Phys. J. C **12** (2000) 375 [hep-ph/9903282].

[24] A. D. Martin, R. G. Roberts, W. J. Stirling and R. S. Thorne, Phys. Lett. B **531** (2002) 216 [hep-ph/0201127].

[25] F. W. Bopp, R. Engel and J. Ranft, "Rapidity gaps and the PHOJET Monte Carlo," hep-ph/9803437.

[26] T. Abe, "GRAPE-Dilepton (Version 1.1): A generator for dilepton production in e p collisions," Comput. Phys. Commun. **136** (2001) 126 [hep-ph/0012029].

[27] B. List and A. Mastroberardino, "DIFFVM: A Monte Carlo generator for diffractive processes in e p scattering", prepared for *Workshop on Monte Carlo Generators for HERA Physics*, Hamburg, Germany, 27-30 Apr 1998.

[28] S. Aid *et al.* [H1 Collaboration], Z. Phys. C **69** (1995) 27 [hep-ex/9509001].

[29] C. F. von Weizsäcker, Z. Phys. **88** (1934) 612;
E. J. Williams, Phys. Rev. **45** (1934) 729;
S. Frixione *et al.*, Phys. Lett. B **319** (1993) 339 [hep-ph/9310350].

[30] C. Adloff *et al.* [H1 Collaboration], Eur. Phys. J. C **24** (2002) 517 [hep-ex/0203011].

[31] S. Chekanov *et al.* [ZEUS Collaboration], Eur. Phys. J. C **50** (2007) 283-297 [hep-ex/0612008].
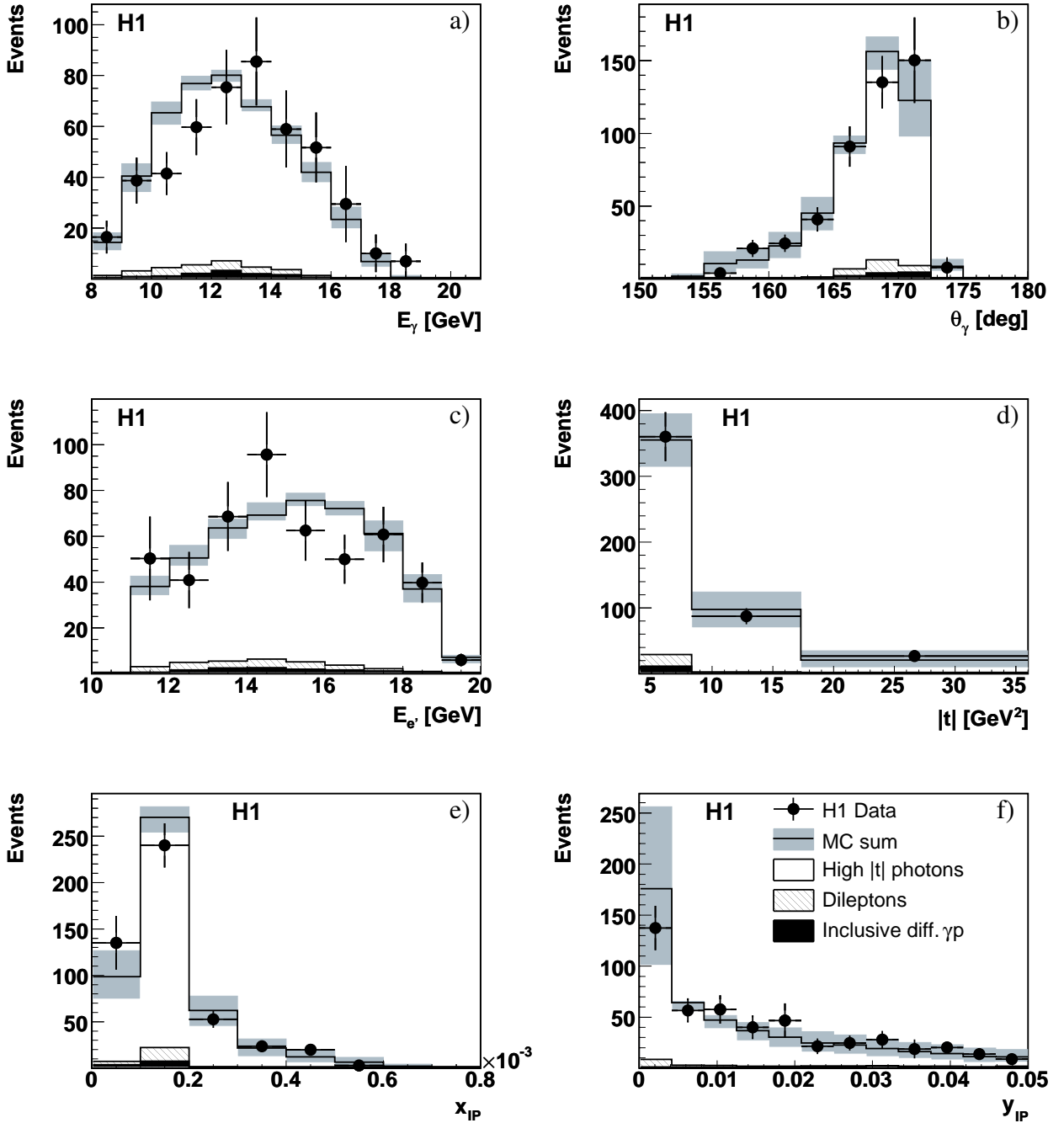
Figure 2: Distributions of the selected events as a function of a) the final state photon energy, b) the final state photon polar angle, c) the scattered positron energy, d) $|t|$, e) $x_{I\!P}$, and f) $y_{I\!P}$. The data corrected for trigger efficiency (black points) are compared with the simulation of diffractive high $|t|$ photons from the weighted HERWIG based on the LLA BFKL calculation (open histogram), and the background from inclusive diffractive photoproduction simulated with PHOJET (full histogram) and dilepton production simulated with GRAPE (hatched histogram). The HERWIG prediction is normalised to the number of data events after background subtraction. The total systematic uncertainty of the simulation is shown by the dark grey shaded band.
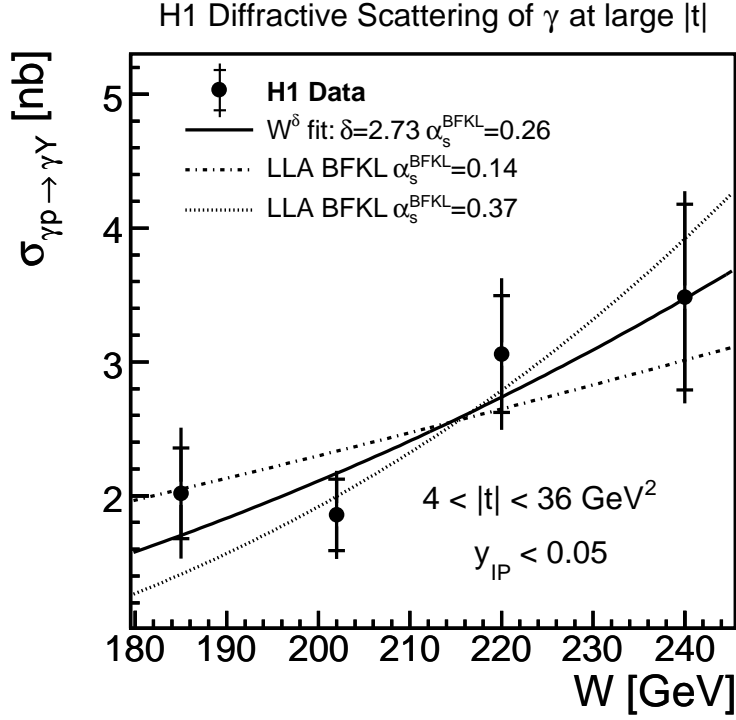
Figure 3: The $\gamma p$ cross section of diffractive scattering of photons as a function of $W$ in the phase space defined by $4 < |t| < 36 \text{ GeV}^2$, $y_{I\!P} < 0.05$ and $Q^2 < 0.01 \text{ GeV}^2$. The average value is $\langle |t| \rangle = 6.1 \text{ GeV}^2$. The inner error bars show the statistical errors and the outer error bars show the statistical and systematic errors added in quadrature. The solid line shows the result of a fit to the cross section of the form $W^\delta$ with $\delta = 2.73 \pm 1.02 \, (\text{stat.})^{+0.56}_{-0.78} \, (\text{syst.})$. This line also corresponds to the LLA BFKL model prediction from the HERWIG event generator with $\alpha_s^{BFKL} = 0.26$. Two additional curves show the LLA BFKL predictions for the additional choices of $\alpha_s^{BFKL} = 0.14$ and $0.37$ corresponding to one standard deviation from the fit value.
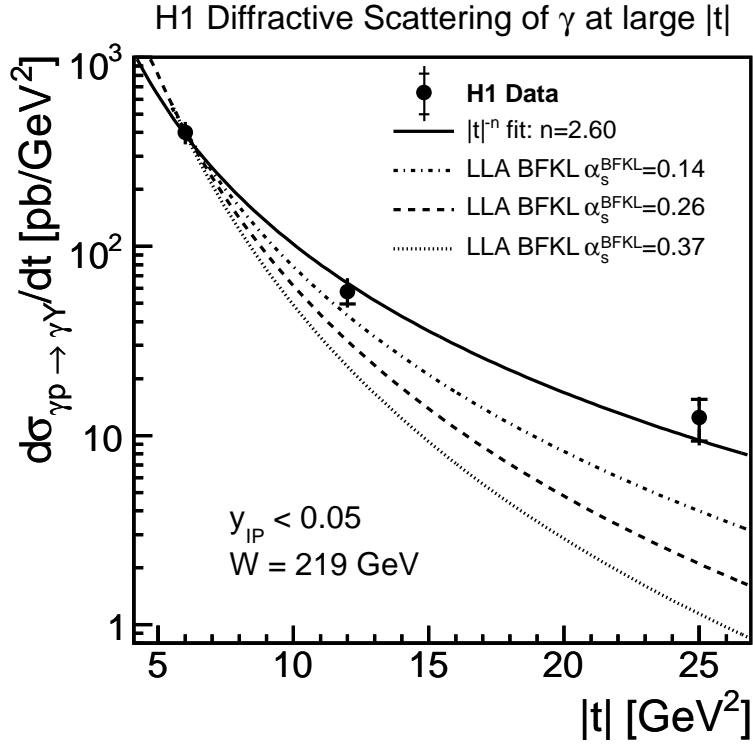
Figure 4: The $\gamma p$ cross section of diffractive scattering of photons differential in $|t|$ for $W = 219$ GeV, $y_{I\!P} < 0.05$ and $Q^2 < 0.01$ GeV$^2$. The inner error bars show the statistical errors and the outer error bars show the statistical and systematic errors added in quadrature. The solid line shows the result of a fit to the cross sections of the form $|t|^{-n}$ with $n = 2.60 \pm 0.19$ (stat.)$^{+0.03}_{-0.08}$ (syst.). Three additional curves show the LLA BFKL model predictions from the HERWIG event generator for the values $\alpha_s^{BFKL} = 0.14, 0.26$ and $0.37$.